Mass-flux-based outlet boundary conditions for the lattice Boltzmann method

J. Stat. Mech. (2009) P06015

(http://iopscience.iop.org/1742-5468/2009/06/P06015)

Journal of Statistical Mechanics: Theory and Experiment
An IOP and SISSA journal

Mass-flux-based outlet boundary conditions for the lattice Boltzmann method

K Mattila[1,2], J Hyväluoma[1] and T Rossi[2]

[1] Department of Physics, University of Jyväskylä, PO Box 35, FI-40014 Jyväskylä, Finland
[2] Department of Mathematical Information Technology, University of Jyväskylä, PO Box 35, FI-40014 Jyväskylä, Finland
E-mail: kemattil@jyu.fi, jarhy@jyu.fi and tro@mit.jyu.fi

Received 28 October 2008
Accepted 2 February 2009
Published 18 June 2009

Online at stacks.iop.org/JSTAT/2009/P06015
doi:10.1088/1742-5468/2009/06/P06015

Abstract. We present outlet boundary conditions for the lattice Boltzmann method. These boundary conditions are constructed with a mass-flux-based approach. Conceptually, the mass-flux-based approach provides a mathematical framework from which specific boundary conditions can be derived by enforcing given physical conditions. The object here is, in particular, to explain the mass-flux-based approach. Furthermore, we illustrate, transparently, how boundary conditions can be derived from the emerging mathematical framework. For this purpose, we derive and present explicitly three outlet boundary conditions. By construction, these boundary conditions have an apparent physical interpretation which is further demonstrated with numerical experiments.

Keywords: fluids in confined geometries, interfacial phenomena and wetting, lattice Boltzmann methods, computational fluid dynamics

1742-5468/09/P06015+14$30.00

Contents

1. Introduction

Physical phenomena encompassing wide spectra of length scales and timescales often pose a challenge for mathematical modelling and numerical simulation. For example, due to limitations on computational resources, only some of the relevant length scales can be typically captured in simulations. Here we are particularly concerned about spatial length scales. More often than not, the spatial domain in a simulation is truncated from the physical domain. Boundaries of truncated simulation domains can be classified into so-called artificial boundaries, not present as such in the physical domain, and into boundaries which represent some physical interface. Artificial boundaries, requiring special conditions, are common when simulating, e.g., waves in physically unbounded domains [1]. Artificial boundaries are common also in computational fluid dynamics. For example, the objective could be to impose a boundary condition at the outlet, which has a minimal influence on the flow field developed inside the domain [2, 3]. These are often referred to as open or free-flow boundary conditions.

Hereafter we focus on flow systems governed by inlets and outlets. Pipe and vessel flows are common examples. In particular, we focus on outlet boundary conditions for the lattice Boltzmann method (LBM). We explain the essence of the so-called mass-flux-based approach [4], and illustrate how it can be applied to derive outlet boundary conditions. The philosophy in the mass-flux-based approach is to enforce a given physical condition at the domain boundary. Most importantly, the physical condition is formulated, and enforced, in such a way that the local velocities have freedom to evolve. From the mathematical perspective, the physical boundary condition here gives an expression for the boundary densities (pressures) after which, and with some fundamental assumptions, local boundary velocities are readily available in the LBM. Since the objective is to enforce a given condition, the outlet boundary conditions presented here are not strictly free-flow conditions—only in close relation to them.

J. Stat. Mech. (2009) P06015

Previous research related to this work includes extrapolation-based boundary conditions for the LBM [5, 6]. There, unknown distribution values are extrapolated at the domain boundaries. These extrapolation-based schemes can be classified as *Neumann* type boundary conditions. In [7] Grad's approximation for the unknown distribution values was utilized. Junk *et al* [8] proposed lattice Boltzmann implementations of several Navier–Stokes outflow boundary conditions. Owing to the premiss, the macroscopic meaning of these implementations is evident.

This paper is composed as follows. Section 2 will explain the mass-flux-based approach for lattice Boltzmann boundary conditions. In the section 3, three outlet boundary conditions are derived by using the mass-flux-based approach. Properties of these boundary conditions are demonstrated with numerical experiments in section 4. Proposed boundary conditions are discussed in section 5 and finally a summary is presented.

2. A mass-flux-based approach for lattice Boltzmann boundary conditions

Complex flow domains may impose major challenges to inlet and outlet boundary conditions. To facilitate simulations with arbitrarily shaped inlets, a mass-flux-based inlet boundary condition for the LBM was recently introduced [4]. The proposed boundary condition operates with minimal amounts of boundary data—the average velocity at the inlet—while producing steady-state velocity fields which faithfully conform to complex inlet geometries. In the current formulation, a unidirectional flow perpendicular to the inlet is assumed. Here our aim is to explain the mass-flux-based approach and to show that it is applicable not only for inlet but also for outlet boundary conditions.

To begin with, we briefly introduce the concepts and notation related to the mass-flux-based approach. For simplicity, let us consider a simple two-dimensional channel flow with an inlet boundary (as depicted on the right-hand side of figure 1). The flow is from left to right and perpendicular to the inlet boundary—as is the pressure gradient. This implies a spatially constant pressure $p_c(t)$ at the boundary. Due to the equation of state of ideal gas, a constant pressure in the LBM implies constant density: $p_c(t) = c_s^2 \rho_c(t)$, where c_s is the speed of sound. The flow gives rise to a mass flux $Q(t)$ through the domain boundary. In particular, in the LBM, it is fruitful to express the total mass flux as the difference of inflowing and outflowing masses: $Q(t) = Q_{in}(t) - Q_{out}(t)$. This is because the outgoing mass can be measured in the LBM at each discrete time step as will be explained below.

In the standard LBM, the spatial domain is discretized with a uniform lattice. Let n_f denote the number of lattice nodes at the boundary. The domain for microscopic velocities is represented, after discretization, with only a small set of velocity vectors—the most startling feature of the LBM. That is, there are b probability distribution functions $f_i(\vec{r}, t), i = 0, \ldots, b-1$, at every lattice site describing the microscopic state at time t, each of them associated with one of the b velocity vectors $\vec{c}_i$ or so-called links. The arrows on the left-hand side of figure 1 represent the values of f_i in the D2Q9 model that is used for illustration ($b = 9$) [9]. Evolution of the dynamic variables f_i is governed by the lattice Boltzmann equation and it proceeds in discrete time steps which are further decomposed into streaming and collision events. We choose the streaming operation to precede the collision, and denote the instant after streaming but before collision by t^* at a time step t. Furthermore, below we shall apply the so-called incompressible version

J. Stat. Mech. (2009) P06015

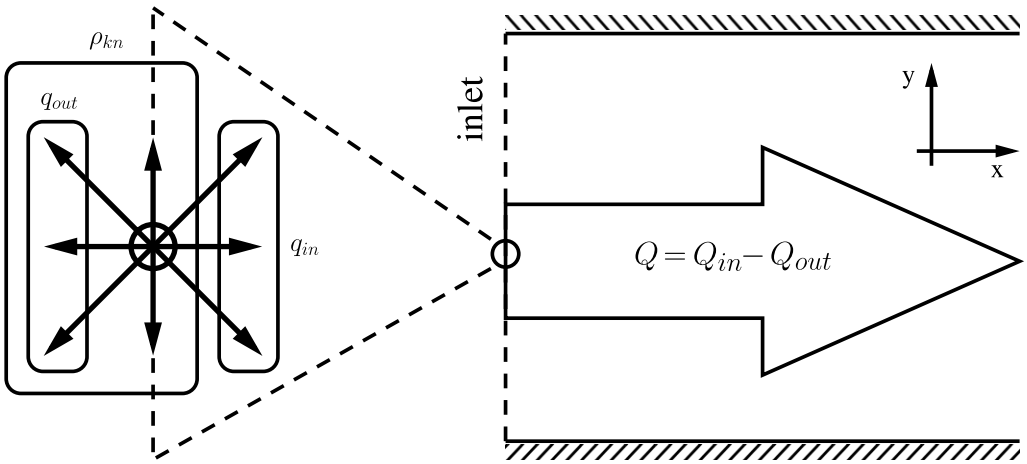

Figure 1. A two-dimensional channel with an inlet boundary. Flow is in the x-direction and perpendicular to the inlet. At the boundary local mass fluxes, q_{in} and q_{out}, are computed from distribution functions associated with the in-bound and out-bound links, respectively.

of the lattice Boltzmann method (ILBM) [10], where the equilibrium function is slightly modified in comparison to the standard one [9]. In the ILBM, the density is decomposed into constant and fluctuating parts, $\rho = \rho_0 + \delta\rho$, the momentum density is redefined as $\rho_0 \vec{u}(\vec{r}, t) = \sum_i \vec{c}_i f_i(\vec{r}, t)$, and all terms proportional to $\delta\rho(\vec{u})$ and $\delta\rho(\vec{u})^2$ are neglected—particularly in the equilibrium part.

At the domain boundaries, some of the links point into the domain and some out of the domain (see figure 1). In our problem formulation, the values of the distribution functions associated with the in-bound links are unknown at t^*. The sum of these values equals $q_{\mathrm{in}}(\vec{r}, t^*)/c$, where we denote the local in-bound mass flux by q_{in}. Here the lattice velocity $c = \Delta x/\Delta t$ is set to unity by selecting $\Delta x = 1$ and $\Delta t = 1$. The sum of the remaining distribution functions is the locally known mass after the streaming, $\rho_{kn}(\vec{r}, t^*)$. The value of the local out-bound mass flux $q_{\mathrm{out}}(\vec{r}, t^*)$ is also known and computed as the product of the sum of the distribution functions associated with the out-bound links and the unit velocity c (see [4] for details). The total inflowing and outflowing masses, $Q_{\mathrm{in}}(t^*)$ and $Q_{\mathrm{out}}(t^*)$, are sums of $q_{\mathrm{in}}(\vec{r}, t^*)$ and $q_{\mathrm{out}}(\vec{r}, t^*)$ over the boundary nodes, respectively. Similarly, $M_{kn}(t^*)$ is the sum of $\rho_{kn}(\vec{r}, t^*)$.

Our mass-flux-based approach is for obtaining the macroscopic variables at the domain boundary. To recapitulate, assumption of a flow perpendicular to the boundary implies $\rho(\vec{r}, t^*) = \rho_{\mathrm{c}}(t^*)$, $\rho_0 u_x(\vec{r}, t^*) = q_{\mathrm{in}}(\vec{r}, t^*) - q_{\mathrm{out}}(\vec{r}, t^*)$, and $u_y(\vec{r}, t^*) = 0$ (also $u_z(\vec{r}, t^*) = 0$ in three-dimensional case). To enforce a common density along the boundary, we must set

$$q_{\mathrm{in}}(\vec{r}, t^*)c^{-1} = \rho_{\mathrm{c}}(t^*) - \rho_{kn}(\vec{r}, t^*). \tag{1}$$

Thus, if we have a value for the common density, we can compute locally the velocity component perpendicular to the boundary. In this sense, the mass-flux-based approach is related to the determination of $\rho_{\mathrm{c}}(t^*)$. Figure 2 depicts the data dependences in the mass-flux-based approach. As is evident, if a value is assigned on some physical grounds

J. Stat. Mech. (2009) P06015

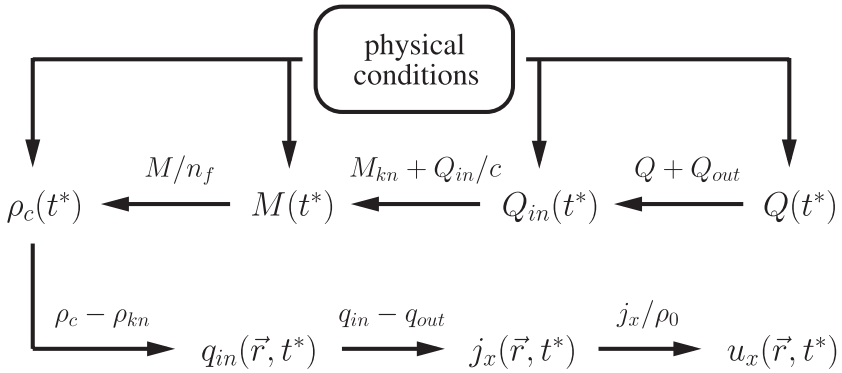

Figure 2. Data dependences in the mass-flux-based approach for inlet and outlet boundary conditions.

to the common density $\rho_c(t^*)$, to the total mass related to the boundary nodes $M(t^*)$, to the total influx of mass $Q_{\text{in}}(t^*)$, or to the total mass flux $Q(t^*)$, values for the remaining three quantities can be computed. It is a matter of convenience or physical situation which one of these four quantities is *a priori* assigned.

For example in [4], the physical condition is to have a given average flow velocity at the inlet (and hence a given Reynolds number): the average velocity is enforced by enforcing a fixed value for the total mass flux Q from which a value is computed for the common density. It is important to note that the value for the common inlet density $\rho_{\text{c}}(t^*)$ is not explicitly fixed. It is a function of time, at each time step it is computed so as to ensure a given total mass flux Q, and it will converge as the system reaches a steady state (see, e.g., figure 5). Here we introduce three boundary conditions for the outlets by following the mass-flux-based approach. Before proceeding to the outlet boundary conditions, we consider how to map macroscopic variables to microscopic ones—a question inherently related to the LBM.

2.1. From known hydrodynamic variables to unknown distribution values

The mass-flux-based approach is for obtaining macroscopic variables at the domain boundary. However from a mathematical point of view, an inlet or an outlet boundary condition is, in the LBM, an expression or equation for the unknown distribution values at the domain boundaries. Figure 3 presents an enumeration of the velocity vectors for the D3Q19 model, applied in our numerical experiments. If an inlet is considered, the unknown distribution values here are $f_{SE}, f_{BE}, f_E, f_{TE}$ and f_{NE}. To formulate an expression for the unknowns, we first decompose the distribution functions into equilibrium, f_i^{eq}, and non-equilibrium, $f_i^{\text{neq}} = f_i - f_i^{\text{eq}}$, parts. The equilibrium part $f_i^{\text{eq}}(\rho, \vec{u})$ is a function of density $\rho(\vec{r}, t)$ and flow velocity $\vec{u}(\vec{r}, t)$ alone [9, 10].

A simple expression for the unknown distribution functions at the boundary is obtained with the bounce-back of the non-equilibrium part:

$$f_i(\vec{r}, t^\star) = f_i^{\text{eq}}(\vec{r}, t^\star; \rho_{\text{c}}, \vec{u}) + f_{-i}^{\text{neq}}(\vec{r}, t^\star), \tag{2}$$

which is in accordance with the first-order Chapman–Enskog expansion [11]. Subscript $-i$ refers to the link $\vec{c}_{-i} = -\vec{c}_i$. Above we have assumed that for each in-bound link

J. Stat. Mech. (2009) P06015

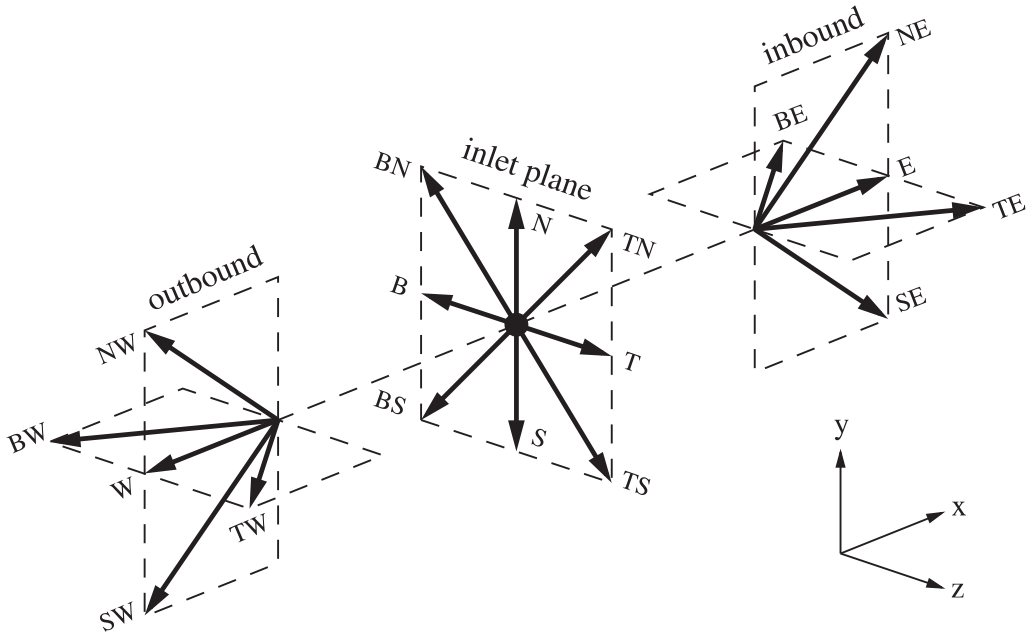

Figure 3. Enumeration of the velocity vectors for the D3Q19 model. The vectors are decomposed into three sets: in-bound, out-bound, and those parallel to the inlet boundary. The filled circle at the inlet plane denotes so-called rest-link or zero-link.

there exists an out-bound link for which the distribution value is known after streaming. Equation (2) is a mapping from macroscopic to microscopic variables, and is actually equivalent to the approach proposed by Zou and He [12] without the correction terms: it will ensure the desired density and momentum perpendicular to the domain boundary.

However, a simple bounce-back of the non-equilibrium part does not ensure desired values for transverse momentum components. In particular, zero momentum along the inlet plane is not guaranteed. Figure 4 presents non-zero transverse velocities. In [4], we applied equation (2) at the inlet and observed divergence of the relative L_2-error norm when $Re \gtrsim 1$. The divergence is related to non-linear dependence of transverse momentum components on the Reynolds number: when $Re \gtrsim 1$, the incorrect momentum along the domain boundary begins to dominate the error (see figure 4). That is, the incorrect equilibrium part becomes the leading source of error. Fortunately, zero momentum along the inlet is guaranteed when the correction terms are included in accordance with [12]:

$$
\begin{aligned}
f_E &= f_W + \tfrac{1}{3}\rho_0 u_x, \\
f_{SE} &= f_{NW} + \tfrac{1}{6}\rho_0 u_x + \tfrac{1}{2}(f_{BN} + f_N + f_{TN} - f_{TS} - f_S - f_{BS}), \\
f_{NE} &= f_{SW} + \tfrac{1}{6}\rho_0 u_x - \tfrac{1}{2}(f_{BN} + f_N + f_{TN} - f_{TS} - f_S - f_{BS}), \\
f_{BE} &= f_{TW} + \tfrac{1}{6}\rho_0 u_x + \tfrac{1}{2}(f_{TS} + f_T + f_{TN} - f_{BN} - f_B - f_{BS}), \\
f_{TE} &= f_{BW} + \tfrac{1}{6}\rho_0 u_x - \tfrac{1}{2}(f_{TS} + f_T + f_{TN} - f_{BN} - f_B - f_{BS}).
\end{aligned}
\tag{3}
$$

By using expressions (3), the divergence of error plaguing our previous implementations is cured: the relative L_2-error norm is almost constant (independent of the relaxation time and average velocity) for a given lattice resolution. Poiseuille-flow

J. Stat. Mech. (2009) P06015

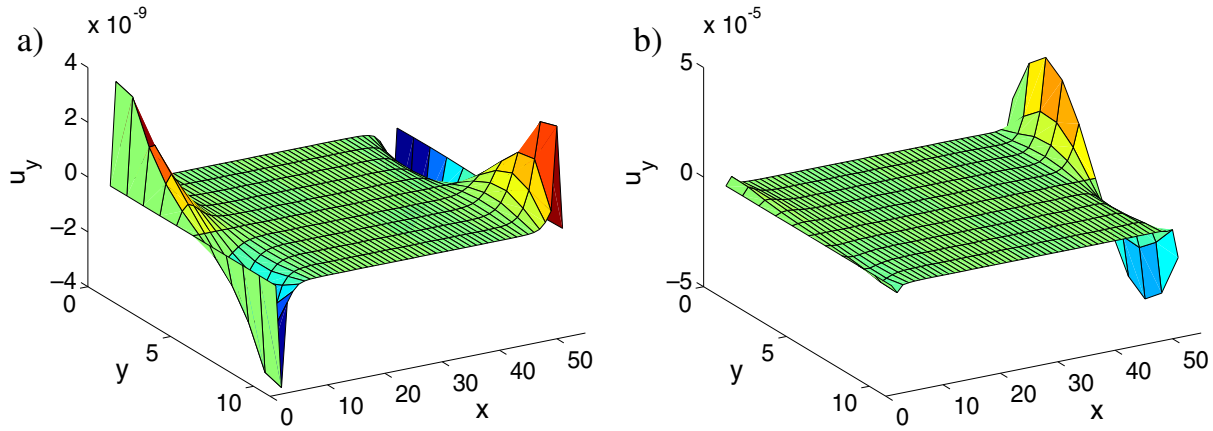

Figure 4. Transverse velocity component u_y in simple channel flow simulations with the D3Q19 model. Channel walls are separated in the y-direction; the distance between walls is 11 lattice units. The flow is in the x-direction: the inlet is at $x = 1$ and the outlet at $x = 51$. Periodic boundary conditions are used in the z-direction. Mass-flux-based boundary conditions in conjunction with the scheme proposed by Zou and He are used, with and without correction terms, at the inlet and outlet, respectively. The relaxation time is set to unity. In (a) average velocity $\bar{u}_x = 0.000\,01$ is enforced at the inlet and outlet ($Re = 0.000\,66$), while in (b) $\bar{u}_x = 0.01$ ($Re = 0.66$). Clearly, u_y has a greater value at the outlet when Re is increased. Note also the non-zero value of u_y close to the inlet.

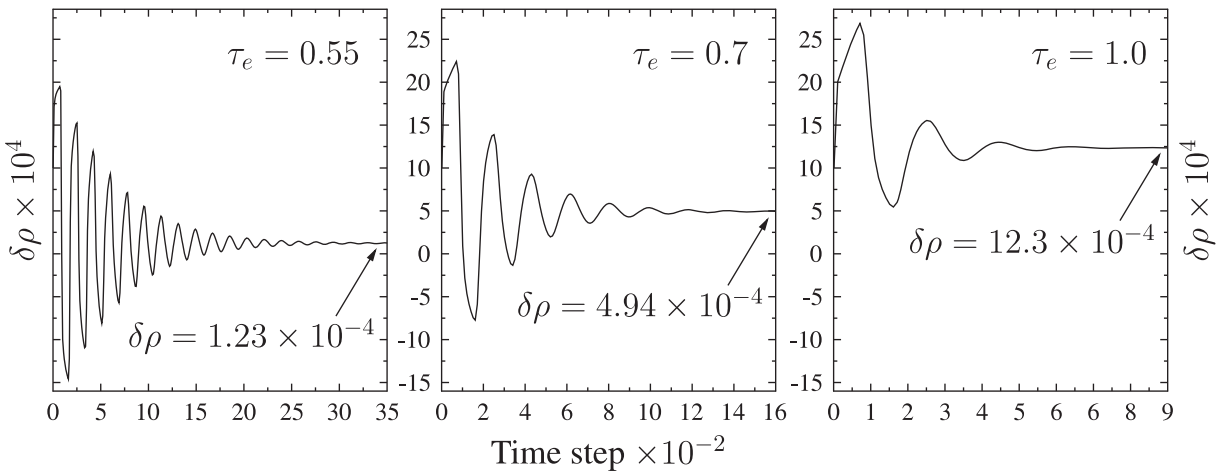

Figure 5. Inlet density deviation from the average value as a function of time in simple channel flow simulations with the D3Q19 model. The channel height is 11 lattice units; average velocity $\bar{u}_x = 0.001$ is enforced at the inlet and outlet. Results are presented with equal scales for three viscosity values: $1/60, 4/60$, and $10/60$. Pressure oscillations, due to the initial and boundary conditions, are evident. With lower viscosity, oscillations have greater amplitude; with higher viscosity, oscillations are quickly damped by viscous dissipation. Steady-state values for the inlet density deviations are also presented: here the convergence to a value, which is proportional to the viscosity, is demonstrated.

J. Stat. Mech. (2009) P06015

simulations were run up to $Re = 115.5$. The above expressions are still not ideal. While transverse momentum components are zero at the domain boundary, they are in general not zero at the adjacent cross-section parallel to the boundary (see figure 4). Expressions (3) do not guarantee that second moments of the non-equilibrium part, related to the strain rate tensor, are consistent with Navier–Stokes equations. Incorrect strain rates force transverse momentum components. In what follows, we apply the scheme proposed by Zou and He with the correction terms in numerical experiments. However, the scheme is not an integral part of the mass-flux-based approach—even more elaborate mappings could be used.

Finally, we make a short comment on the time evolution of the system to the steady state. During transient phases, we observe pressure oscillations. Figure 5 illustrates oscillations observed in simple channel flow simulations. The main sources for oscillations are crude initial conditions [13, 14]. We initialize distribution functions with equilibrium parts using uniformly zero velocity and average density. The discrepancy between initial and domain boundary conditions results in an impulse to the system when the time iteration is started. The lifetime of the oscillations may be further prolonged by domain boundary conditions [13]. For example, a mass-flux-based approach in conjunction with the expressions (3) has two feedback mechanisms contributing to the oscillations. First, computation of e.g. the common inlet density $\rho_c(t^*)$ is dependent on the flow field developed at the interior of the domain. Secondly, the expressions (3) explicitly include distribution values propagating from the interior of the domain. However, stability issues related to these two mechanisms are not further explored here.

3. Outlet boundary conditions

Since our interest ultimately lies in the simulation of flow in tumour vascular systems, we focus on flow domains involving multiple outlets. Although the outlet boundary conditions are presented here, for the sake of simplicity, in a system with a single inlet branching to two outlets (cf figure 6), they can be straightforwardly generalized to systems with an arbitrary number of outlets. In what follows, superscripts (0), (1), and (2) are associated with the inlet and with the two outlets, respectively. For example, $p^{(0)}$ is the pressure at the inlet, $u^{(1)}_{\max}$ is the maximum velocity at the outlet 1, and $Q^{(2)}$ is the total mass flux through the outlet 2. Again, we assume a unidirectional flow at the domain boundaries. To be exact, we assume $u^{(i)}_x \geq 0$ and $u^{(i)}_y = u^{(i)}_z = 0$ at the boundaries. Furthermore, in each of the three boundary conditions described below, we require the total mass flow through all the domain boundaries to vanish, that is

$$\begin{aligned} Q^{(0)}(t^*) &= Q^{(1)}(t^*) + Q^{(2)}(t^*) \\ &= (Q^{(1)}_{\text{out}}(t^*) - Q^{(1)}_{\text{in}}(t^*)) + (Q^{(2)}_{\text{out}}(t^*) - Q^{(2)}_{\text{in}}(t^*)), \end{aligned} \tag{4}$$

which ensures the mass conservation in the system.

To begin with, we present an obvious boundary condition where a portion of the inlet mass flux is on some basis *a priori* assigned for the outlets:

$$Q^{(1)}(t^*) = \Delta Q^{(0)}(t^*), \qquad Q^{(2)}(t^*) = (1-\Delta)Q^{(0)}(t^*), \qquad \Delta \in [0,1]. \tag{5}$$

Above, the physical condition or expression which determines $\Delta(t^*)$ is the only non-trivial element. Actually, the two following boundary conditions can be formulated as

J. Stat. Mech. (2009) P06015

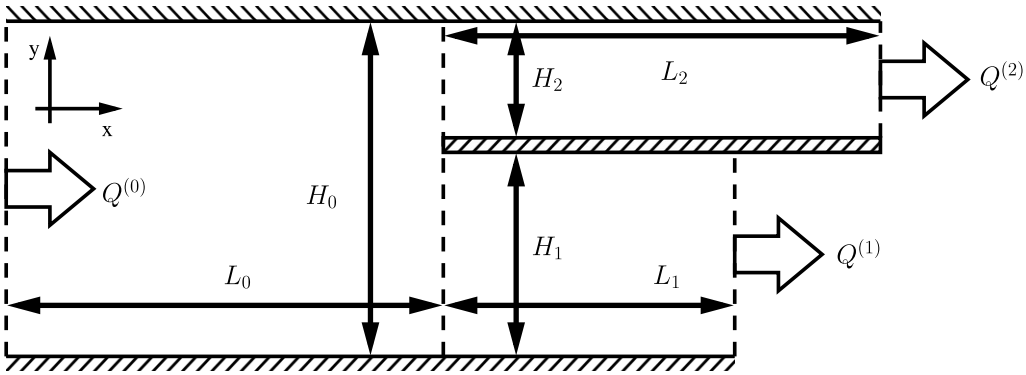

Figure 6. A channel geometry with one inlet and two outlets. The inlet is on the left and the outlets are on the right. The benchmark geometry includes three walls, one of which divides the flow into two branches.

equation (5) with a specific expression for $\Delta(t^*)$. In our opinion, however, it is more fruitful and intuitive to consider those two boundary conditions independently.

In the second boundary condition, we enforce a given ratio between densities (pressures) at the outlets, i.e., $\rho_c^{(2)}(t^*) = \alpha\rho_c^{(1)}(t^*)$, where $\alpha \geq 0$. Here, for simplicity, we consider the case with equal densities at the outlets ($\alpha = 1$). By using this condition in equation (4), together with equation (1), we can obtain an expression for the density:

$$\rho_c^{(1)}(t^*) = \frac{1}{(n_f^{(1)} + n_f^{(2)})}(-Q^{(0)}(t^*)/c + Q_{\text{out}}^{(1)}(t^*)/c + Q_{\text{out}}^{(2)}(t^*)/c + M_{kn}^{(1)}(t^*) + M_{kn}^{(2)}(t^*)). \quad (6)$$

Since everything on the right-hand side of equation (6) can be measured after streaming, we have a time-dependent expression for the outlet densities. The procedure presented in the previous section is then utilized to enforce these densities. It is important to note, that we do not enforce any particular values for the outlet densities: we simply enforce a specific ratio between the outlet densities.

The third boundary condition enforces a given ratio between pressure gradients at the outlets. In the LBM, it is equivalent to enforce $\partial_x(\rho_c^{(2)}(t^*)) = \alpha\partial_x(\rho_c^{(1)}(t^*))$, where $\alpha \geq 0$. Again, here we require $\alpha = 1$ for simplicity. By applying first-order finite-difference approximation for the derivatives, we get $\rho_c^{(2)}(t^*) - \widehat{\rho}_2(t^*) = \rho_c^{(1)}(t^*) - \widehat{\rho}_1(t^*)$, where $\widehat{\rho}_2$ and $\widehat{\rho}_1$ are average densities after streaming measured from the cross-sections adjacent to the outlets 2 and 1, respectively. With this approximation we can obtain, from equation (4), an expression for the density:

$$\begin{aligned}\rho_c^{(1)}(t^*) = \frac{1}{(n_f^{(1)} + n_f^{(2)})}(&- Q^{(0)}(t^*)/c + Q_{\text{out}}^{(1)}(t^*)/c + Q_{\text{out}}^{(2)}(t^*)/c \\ &+ M_{kn}^{(1)}(t^*) + M_{kn}^{(2)}(t^*) + n_f^{(2)}\widehat{\rho}_1(t^*) - n_f^{(2)}\widehat{\rho}_2(t^*)). \end{aligned} \quad (7)$$

The second and third boundary conditions appear very similar, especially when comparing their mathematical manifestations, i.e., equations (6) and (7). However, the physical conditions leading to these equations are fundamentally different: a fact which is evident from simulated flow fields. This will be demonstrated in section 4.

J. Stat. Mech. (2009) P06015

4. Numerical experiments

The first boundary condition, equation (5), is from our perspective a generic formulation: the physics involved is hidden behind the expression for $\Delta(t^*)$. Here we focus on the other two boundary conditions, equations (6) and (7), which are specific and physically self-evident. We use numerical simulations to showcase these two boundary conditions in operation. For the simulations, we constructed a three-dimensional channel geometry with one inlet and two outlets. The geometry is presented in figure 6, where the inlet is on the left and the outlets are on the right. The flow is in the x-direction and the channel walls are separated in the y-direction. The redundant z-direction is included in order to demonstrate the boundary conditions with the D3Q19 model [9].

The channel geometry is composed of three walls, one of which bifurcates the flow into two branches: in figure 6 outlet channel 1 is the lower branch and outlet channel 2 is the upper branch. There are two parameters for controlling the geometry. Parameter h is the relative height of the outlet channels, i.e., $h = H_1/(H_1+H_2)$, and L_1 determines the length of channel 1. Other parameters are fixed: $L_0 = L_2 = 1000$, $H_0 = 101$, and $H_1 + H_2 = 100$. Relatively long channels are used to ensure unidirectional and perpendicular flows at the domain boundaries. The size of the domain in the z-direction is 1. All the values given in this section are in dimensionless lattice units. The inlet mass flux $Q^{(0)}$ is fixed with average velocity $\bar{u}_x^{(0)} = 10^{-5}$ [4].

A periodic boundary condition is applied in the z-direction and a no-slip condition at the solid–fluid interfaces is enforced by the standard halfway bounce-back boundary condition [15, 16]. That is, the solid–fluid interfaces are located exactly halfway between adjacent lattice nodes. Furthermore, a two-relaxation-time scheme, in which the distribution function is decomposed into symmetric (even) and anti-symmetric (odd) parts and relaxed with separate relaxation parameters, is utilized [11]: the relaxation time τ_e is for tuning the viscosity and the other relaxation time τ_o is chosen so as to minimize the viscosity dependence of the slip velocity (see [11] for details). Here we use $\tau_\mathrm{e} = 1$. Simulations are iterated in time until a steady state is reached.

4.1. Equal pressure at the outlets

The benchmark geometry presented in figure 6 gives rise to non-trivial flows. In particular, in the vicinity of the bifurcation point, $x = 1000$, flow diverges into two branches and exhibits transverse velocity component u_y (see the inset in figure 7). Also, when equal pressures or equal pressure gradients are enforced at the outlets, there is a pressure build-up at the entrance of the smaller outlet channel. This build-up is enhanced by the relative size difference between the two channels. Transverse velocity and pressure build-up are just two properties of a complex flow. To the best of our knowledge, there are no analytical solutions available for describing the complete velocity (or pressure) field in this kind of a geometry.

It is not our primary concern to investigate the flow properties in more detail. Here we rather concentrate on the properties of the proposed boundary conditions. Figure 7 presents simulation results when equal pressures are enforced at the outlets, parameter h varies between 0.5 and 0.9, and $L_1 = 1000$. Values of $\delta\rho$, i.e., the density deviation from the average value ρ_0, and the transverse velocity component are presented along the channel;

J. Stat. Mech. (2009) P06015

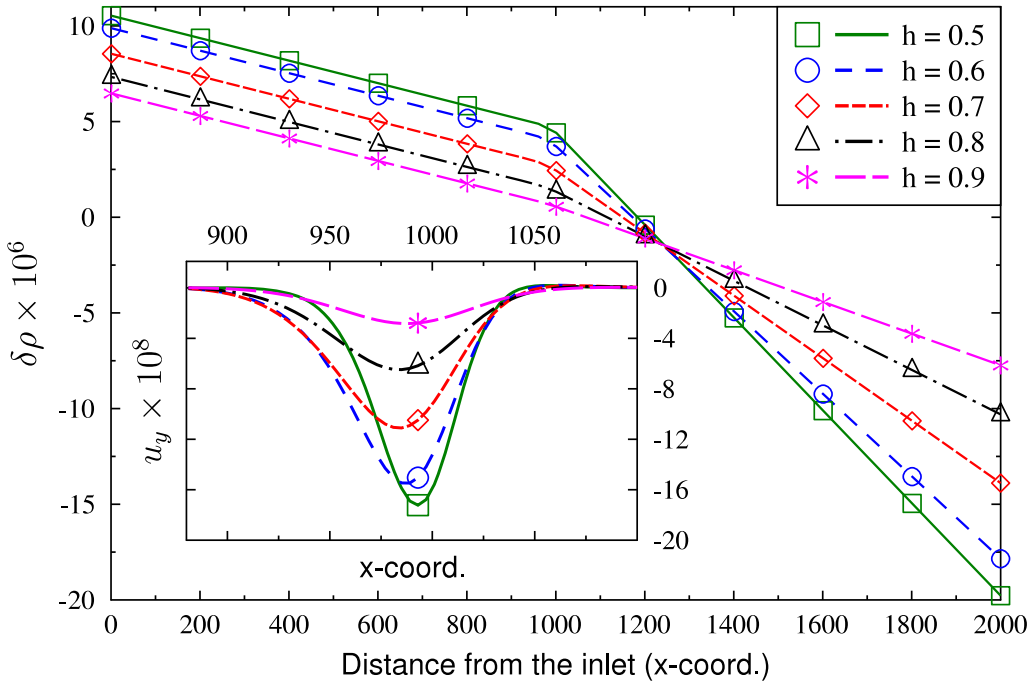

Figure 7. Density deviation from the average value in simulations where equal densities were enforced at the outlets, $0.5 \leq h \leq 0.9$, and $L_1 = 1000$. The inset shows the transverse velocity component near the bifurcation point. Values are measured close to the lower wall ($y = 6$).

values are measured through outlet channel 1 along a line close to the lower wall ($y = 6$). Figure 7 reveals that the density gradient is constant at the inlet channel and is unaffected by the variation of parameter h as expected. The density gradient is constant also at the outlet channel, but the value depends on h. In the region close to the bifurcation point, the density gradient is not a constant as it assumes a new value. In addition, close to the bifurcation point, the flow has transverse velocity as depicted in the inset. Figure 7 also confirms that the absolute value of the density (pressure) is not fixed at the inlet or at the outlet: densities are free to adapt to the given physical conditions. Furthermore, figure 8 emphasizes the major feature of mass-flux-based boundary conditions: the velocity field adapts to the geometries even at the domain boundaries. For example here, it is apparent that the velocity field has evolved to the correct parabolic profile both at the inlet and at the outlets, even though this information is not explicitly given.

4.2. Equal pressure gradients at the outlets

Now we proceed to the boundary condition where equal pressure (density) gradients are enforced at the outlets. This case is particularly interesting since a more quantitative evaluation of the boundary condition is feasible. By additionally assuming, together with equation (4) and $\partial_x(\rho_c^{(2)}(t^*)) = \alpha\partial_x(\rho_c^{(1)}(t^*))$, separate steady-state Poiseuille solutions for flows between two plates at the inlet and outlets, we are in a position to compute some analytical results relating quantities at the outlets to those at the inlet. Let β denote

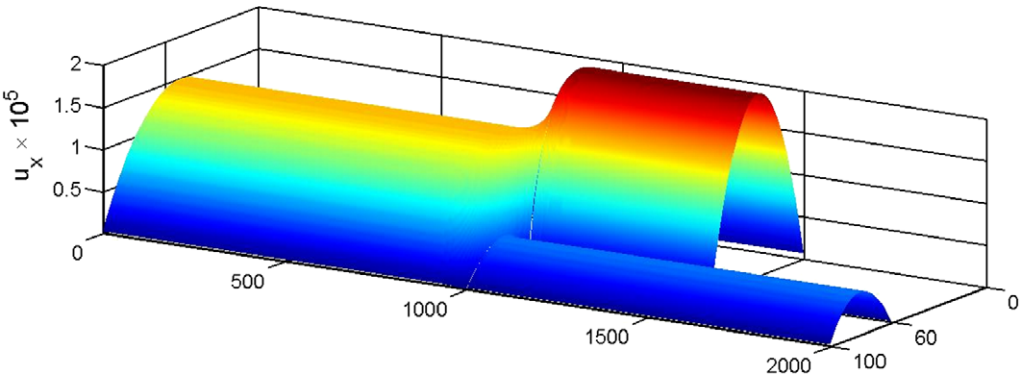

Figure 8. Value of the velocity component u_x in a simulation where equal densities were enforced at the outlets. The geometric parameters were $h = 0.6$ and $L_1 = 500$. A parabolic velocity profile is evident (except at the vicinity of the bifurcation point).

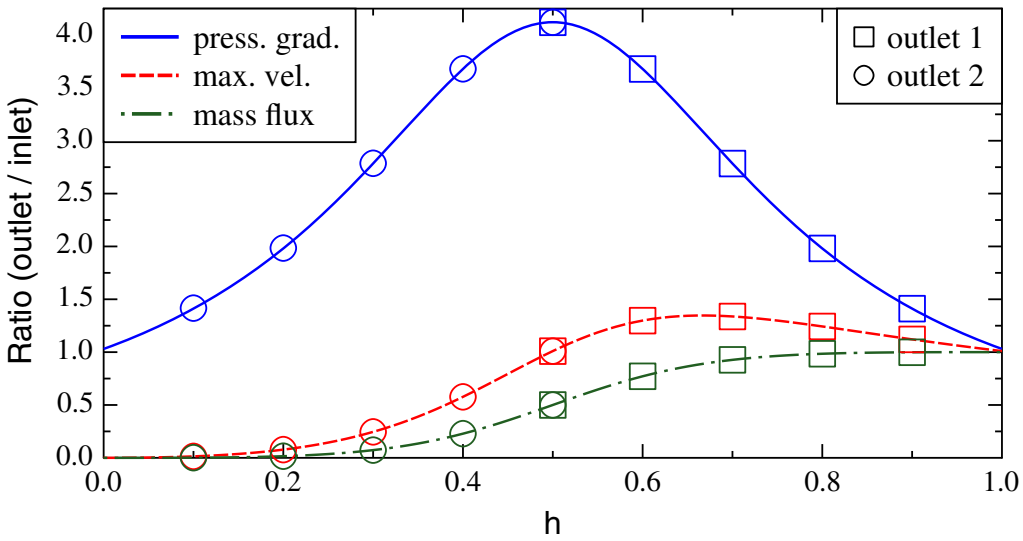

Figure 9. Relative values of quantities when equal density gradients were enforced at the outlets. Symbols denote values measured from a simulation series where $0.5 \leq h \leq 0.9$ and $L_1 = 500$. Squares and circles represent values measured from the outlets 1 and 2, respectively. Lines represent analytical ratios.

the ratio between the inlet area and the total outlet area: here $\beta = 101/100$. After some algebra, we obtain expressions for the outlet quantities:

$$\partial_x(\rho_c^{(1)}) = \frac{\beta^3}{h^3 + \alpha(1-h)^3}\partial_x(\rho_c^{(0)}), \qquad u_{\max}^{(1)} = \frac{\beta h^2}{h^3 + \alpha(1-h)^3}u_{\max}^{(0)},$$

$$Q^{(1)} = \frac{h^3}{h^3 + \alpha(1-h)^3}Q^{(0)}.$$

The above expressions relate quantities at the outlets to those at the inlet by defining a ratio between them. In figure 9 we compare ratios measured from a simulation series against ratios computed from the analytical expressions and find a good agreement.

Simulations were done by varying parameter h between 0.5 and 0.9 while $L_1 = 500$. Lines represent analytical ratios and symbols are from simulations: values denoted by squares are measured from the outlet 1 whereas circles are from the outlet 2.

5. Discussion

Numerical methods directly solving Navier–Stokes equations often utilize open boundary conditions at the outlets which are of *Neumann* type or so-called convective boundary conditions (CBC). For example [2, 3], advocate the use of CBC since this has a demonstrated capability to pass travelling stream vortices over the outlet boundary relatively undamaged. In the mass-flux-based approach, values for the hydrodynamic variables, here ρ and $\vec{u}$, are provided at the domain boundaries. The values are provided in such a way that given physical conditions are satisfied. From this perspective, the mass-flux-based approach can be categorized as a *Dirichlet* type boundary condition (cf equations (6) and (7)). The mass-flux-based approach is devised with stationary steady-state flows in mind, rather than for developing transient flows. However, it would be a relevant study to investigate how a mass-flux-based approach copes, e.g., with travelling vortices.

In this work, we have used a mass-flux-based approach to determine densities, constant along the boundary, at the inlet and at the two outlets. To recapitulate, if the density is known, the local velocity perpendicular to the boundary is readily available from equation (1) and the value zero is enforced for the transverse velocity components with expressions (3). Thus, there are three unknown boundary densities, at each discrete time step, for which we assign values with the *Dirichlet* type boundary condition. The density for the inlet is computed so as to enforce a given average velocity. For the outlets we have one equation, here equation (4), to ensure conservation of mass in the system. Additionally, in a general geometry with N outlets, we have $N - 1$ equations describing ratios between pressures or pressure gradients at the outlets (here $N = 2$). That is, we have equal numbers of unknowns and equations for the outlets. Solutions for the outlet densities are presented in equations (6) and (7) enforcing equal pressure and equal pressure gradients, respectively.

The choice of providing expressions for the macroscopic variables at the domain boundaries leads to a difficulty in the LBM: a mapping from macroscopic variables to distribution functions is necessary. The mapping utilized here, equation (3), is not an integral part of the mass-flux-based approach. More elaborate mappings could be used, e.g. mappings which approximate non-equilibrium parts with partial derivatives of the flow velocity [11, 17, 18]. However, accurate approximation of derivatives at the domain boundaries and in arbitrary geometries is a challenge. In addition, the scheme proposed by Zou and He [12] is appealing as it relies only upon local information available at a single lattice node. Comparison of mappings in the context of inlet or outlet boundary conditions, for example with numerical experiments, could produce interesting results.

We have presented schemes to impose given ratios between pressures or pressure gradients at the outlets when using the LBM for numerical simulations. Alternatively, a relation between flow rates or total mass fluxes at the outlets can be imposed. The above cases demonstrate the construction of outlet boundary conditions with the mass-flux-based approach—other boundary conditions are also feasible with the approach. Physical

J. Stat. Mech. (2009) P06015

motivations for the outlet boundary conditions are not considered here. Applications to flows in vascular systems or arteries are particularly appealing [19, 20]. A formulation of a mass-flux-based approach with unidirectional boundary flow, but not perpendicular to the boundary plane, is to be pursued in the future.

6. Summary

We have considered a so-called mass-flux-based approach in the formulation of outlet, as well as inlet, boundary conditions for the LBM. This work is in relation to artificial or open boundary conditions common in conventional CFD. Here we focused on explaining the mass-flux-based approach. In addition, we have illustrated how this approach can be used to derive boundary conditions. The three outlet boundary conditions presented are the concrete outcome of the above illustration. One of the boundary conditions presented is generic and the other two enforce equal density and equal density gradient at the outlets, respectively. The two specific boundary conditions were demonstrated in operation via numerical experiments. Qualitative results were presented for the equal density condition. More quantitative analysis was presented for the equal density gradient condition: with additional assumptions, analytical expressions were obtained relating quantities at the inlet to those at the outlets. Quantities obtained from simulated flow fields were found to be in good agreement with the analytical relations.

References

[1] Berenger J-P, 1996 *J. Comput. Phys.* **127** 363
[2] Sohankar A, Norberg C and Davidson L, 1998 *Int. J. Numer. Methods Fluids* **26** 39
[3] Ol'shanskii M A and Staroverov V M, 2000 *Int. J. Numer. Methods Fluids* **33** 499
[4] Mattila K, Hyväluoma J, Folarin A A and Rossi T, 2008 *Int. J. Numer. Methods Fluids* submitted
[5] Maier R S, Bernard R S and Grunau D W, 1996 *Phys. Fluids* **8** 1788
[6] Chen S, Martínez D and Mei R, 1996 *Phys. Fluids* **8** 2527
[7] Chikatamarla S S, Ansumali S and Karlin I V, 2006 *Europhys. Lett.* **74** 215
[8] Junk M and Yang Z, 2008 *Prog. Comput. Fluid Dyn.* **8** 38
[9] Qian Y H, d'Humières D and Lallemand P, 1992 *Europhys. Lett.* **17** 479
[10] He X and Luo L-S, 1997 *J. Stat. Phys.* **88** 927
[11] Ginzburg I and d'Humières D, 2003 *Phys. Rev.* E **68** 066614
[12] Zou Q and He X, 1997 *Phys. Fluids* **9** 1591
[13] Yu D, Mei R and Shyy W, 2005 *Prog. Comput. Fluid Dyn.* **5** 3
[14] Mei R, Luo L-S, Lallemand P and d'Humières D, 2006 *Comput. Fluids* **35** 855
[15] Wolfram S, 1986 *J. Stat. Phys.* **45** 471
[16] Lavallée P, Boon J P and Noullez A, 1991 *Physica* D **47** 233
[17] Skordos P A, 1993 *Phys. Rev.* E **48** 4823
[18] Latt J and Chopard B, 2008 *Phys. Rev.* E **77** 056703
[19] Grinberg L, Anor T, Madsen J, Yakhot A and Karniadakis G, 2009 *Clin. Exp. Pharmacol. Physiol.* **36** 194
[20] Grinberg L and Karniadakis G, 2008 *Ann. Biomed. Eng.* **36** 1496

J. Stat. Mech. (2009) P06015